RSC Advances

PAPER

View Article Online
View Journal | View Issue

Cite this: *RSC Adv.*, 2017, **7**, 14832

Fabrication of graphitic-C_3N_4 quantum dots coated silicon nanowire array as a photoelectrode for vigorous degradation of 4-chlorophenol

Yan Su,[a] Bo Sun,[a] Shuo Chen,[b] Hongtao Yu*[b] and Jing Liu[a]

Although Si is a successful photovoltaic material, its application in the photoelectrochemical (PEC) field is limited because an insulated SiO_2 layer always extends quickly from surface to depth once bare Si contacts with an aqueous solution. To inhibit this oxidation passivation, Si nanowires (SiNWs) were coated with graphitic-C_3N_4 quantum dots (g-C_3N_4 QDs) to form SiNWs@g-C_3N_4 QDs, in which g-C_3N_4 QDs acted as a protection layer to isolate Si from water and to improve the photogenerated charge transfer. Observed by SEM and TEM, it was confirmed that dispersive g-C_3N_4 QDs anchored on the surface of SiNWs. PEC performance indicated that the photocurrent of bare SiNWs declined obviously while the photocurrent of SiNWs@g-C_3N_4 QDs was stable. The photocurrent of SiNWs@g-C_3N_4 QDs reached 6.7 mA cm^{-2} at −1.5 V (*vs.* SCE) which was 1.6 times higher than that of pristine SiNWs (4.2 mA cm^{-2}). Taking 4-chlorophenol as a target pollutant to investigate the photoelectrocatalytic capability of the SiNWs@g-C_3N_4 QDs, more than 85% of 4-chlorophenol was successfully removed in 120 min, while the value for SiNWs was only 52.0%. The pseudo-first-order kinetic constant of 4-chlorophenol degradation on SiNWs@g-C_3N_4 QDs was 2.3 times as great as that on pristine SiNWs. The improved degradation efficiency benefited from the improved stability as well as the enhanced photo-generated charge transfer and separation driven by the built-in electric field at the interface between g-C_3N_4 QDs and SiNWs. The SiNWs@g-C_3N_4 QDs will also be useful in other research areas such as water splitting, sensors, *etc.*

Received 16th January 2017
Accepted 1st March 2017

DOI: 10.1039/c7ra00671c

rsc.li/rsc-advances

1. Introduction

Due to its non-toxicity, low cost, wide absorption spectra and good electric conductivity, silicon is considered to be an ideal semiconductor material to convert solar energy into chemical energy.[1,2] However, once Si is exposed to moist air or in aqueous conditions,[3] an oxide layer will form to obstruct the charge transfer from Si to aqueous solution. As a result, its ability for photoenergy conversion is turned off.[4] Hence, research has been carried out to inhibit surface passivation of Si *via* appropriate surface modification. At present, various protective layer materials have been investigated intensively, including two-dimensional (2D) layered materials, such as graphene;[5–7] One-dimensional (1D) nanowire materials, such as carbon nanotubes,[8,9] ZnO nanowires.[10] Compared to 2D and 1D materials, the 0D quantum dots (QDs) have small sizes, which can coat Si materials closely and protect Si from oxidation with a thinner cladding layer. Benefitting from these merits, QDs have been further highlighted and shown attractive potential for protective materials. Many QDs materials have been reported as protective layers for Si-based materials, such as CdTe quantum dots[11] and noble-metal nanoparticles (such as Au,[12,13] Ag,[14,15] Pt[16]). Nevertheless, the chalcogen group compounds are toxic and unstable; the noble metal has poor optical transparency and expensive price. Compared to the QDs mentioned above, the metal free graphite carbon nitride (g-C_3N_4) QDs is a more promising candidate. g-C_3N_4 is earth abundant and has excellent response to visible light.[17] Benefited from the strong covalent bond between carbon and nitride atoms,[18] g-C_3N_4 exhibits a superior photocorrosion resistance. In our previous work,[19] 2D g-C_3N_4 nanosheets have been testified to be a proper protection material for Si. Compared with 2D g-C_3N_4, the strong quantum confinement of g-C_3N_4 QDs may arouse more effective optical absorption, and its small size will bring more active site expose effects.[20] Besides, QDs can achieve a coating for arbitrary shape of nanomaterials. Obviously, protecting SiNWs with g-C_3N_4 QDs is a better choice than the reported protection materials.

In this paper, we firstly deposited g-C_3N_4 QDs on the surface of SiNWs to fabricate SiNWs@g-C_3N_4 QDs using a facile dipping method. Then we investigated the photoresponse ability and photoelectrochemical stability of SiNWs@g-C_3N_4 QDs in aqueous solution. At last, the photoelectrocatalytic capability of

[a]*Faculty of Chemical, Environmental and Biological Science and Technology, School of Chemistry, Dalian University of Technology, Dalian 116024, China*

[b]*Key Laboratory of Industrial Ecology and Environmental Engineering, Ministry of Education, School of Environmental Science and Technology, Dalian University of Technology, Dalian 116024, China. E-mail: yuhongtao@dlut.edu.cn*

SiNWs@g-C_3N_4 QDs was evaluated *via* the degradation of 4-chlorophenol. The aim of work is to explore the function of g-C_3N_4 QDs for inhibiting the oxidation passivation and enhancing charge separation of Si materials.

2. Experimental

2.1 Preparation method

SiNWs were prepared by Ag-assisted electroless chemical etching method.[21,22] Clean Si wafer (B-doping p type, ⟨100⟩ orientation, 1–10 Ω cm resistivity, 500 μm thickness with single-side polished) was etched in aqueous solution including 0.005 M $AgNO_3$ and 4.2 M HF. The etching duration was changed to control the length of nanowires. After etching, samples were immersed into the mixture of HNO_3 and H_2O (1 : 1 in volume) and 5% HF solution to remove Ag particles and oxide layer, respectively, and then samples were dried in N_2 flow immediately.

The g-C_3N_4 QDs were fabricated by a chemical stripping method reported by Zhang *et al.*[23] Briefly, bulk g-C_3N_4 was treated in the acid mixture of H_2SO_4 and HNO_3 for about 2 h at room temperature to change into porous g-C_3N_4. Then, the as-prepared porous g-C_3N_4 was exfoliated into ultrathin nanosheet with $NH_3 \cdot H_2O$ by hydrothermal treatment. At last, the g-C_3N_4 QDs were fabricated *via* the ultrasonication of porous g-C_3N_4 nanosheet in ethanol. The as-prepared g-C_3N_4 QDs were deposited onto SiNWs *via* a dipping process followed by an annealing step under 300 °C for 30 min in a N_2 flow. The schematic diagram of the preparation process was shown as Fig. 1.

2.2 Characterization and measurement

The morphologies of samples were observed by scanning electron microscopy (SEM, Hitachi S-4800) and transmission electron microscope (TEM, Tecnai F30). X-ray photoelectron spectroscopy (XPS, ESCALAB 250, Thermo VG) was performed to analyse oxidation states and surface chemical composition of samples. The C 1s signal was set to 284.8 eV for calibration. The PEC performance was tested in a three-electrode cell connecting with a CHI 660 electrochemical station (CH Instruments, Shanghai Chenhua, China). The SiNWs@g-C_3N_4 QDs, a Pt plate and a saturated calomel electrode (SCE) acted as working electrode (effective area 1.0 cm^2), counter electrode and reference electrode, respectively. A high-pressure xenon arc lamp (CHF-XM-500W, Beijing Changtuo, China) was used as light source. All the tests were performed in 0.5 M H_2SO_4 aqueous solution under ambient conditions.

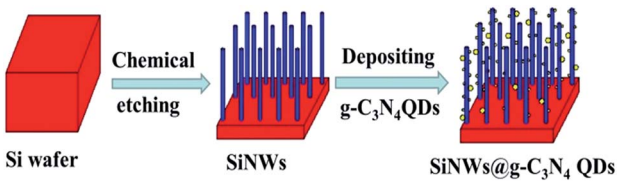

Fig. 1 The schematic diagram of the preparation process of SiNWs@g-C_3N_4 QDs. SiNW was represented by blue column, and the g-C_3N_4 QDs were represented by yellow balls.

2.3 Photoelectrocatalytic degradation of 4-chlorophenol

The photoelectrocatalytic activity of the SiNWs@g-C_3N_4 QDs was evaluated by the degradation of 4-chlorophenol in aqueous solution under xenon lamp irradiation. The light intensity was 100 mW cm^{-2}. During the photoelectrocatalytic reaction, samples were collected at intervals of 10 min for analysis. The concentration of 4-chlorophenol was examined by High Performance Liquid Chromatography (HPLC, Waters 2695, Photodiode Array Detector 2996).

3. Results and discussion

3.1 Sample characterization

The morphology and structure are the foundational information for estimating the physicochemical property of materials. The prepared samples were observed with SEM and the results were displayed in Fig. 2. As anticipation, the length of SiNWs prolonged with the increase of the etching duration. The SiNWs length with etching times of 3 min, 5 min, 10 min and 20 min were 500 nm, 2 μm, 4 μm and 7 μm, respectively. The samples were accordingly named by the length of nanowires as SiNWs-0.5, SiNWs-2, SiNWs-4 and SiNWs-7.

Fig. 3a was high-resolution TEM image of g-C_3N_4 QDs. The picture showed that the average size of quantum dots was ~5 nm. The clear lattice fringes with d = 0.336 nm was found from inset of Fig. 3a, which was consistent with crystalline structures (002) of the reported g-C_3N_4 QDs materials (JCPDS 87-1526). High-resolution TEM image of SiNWs (Fig. 3b) revealed that some nanopores appeared in pristine wires and the diameters were found about 10 nm from inset of Fig. 3b. The morphologies of SiNWs@g-C_3N_4 QDs are shown in Fig. 3c. It displayed that g-C_3N_4 QDs were deposited on the surface of SiNWs structure, indicating that SiNWs@g-C_3N_4 QDs composite was successfully constructed. Besides, as reported in our previous work,[22] some nanopores also appeared on the surface of SiNWs@g-C_3N_4 QDs.

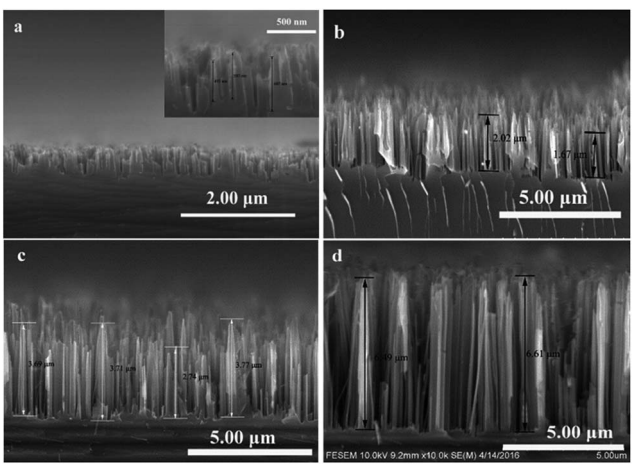

Fig. 2 SEM images of profiles of (a) SiNWs-0.5 (inset: scale bar 500 nm), (b) SiNWs-2, (c) SiNWs-4 and (d) SiNWs-7.

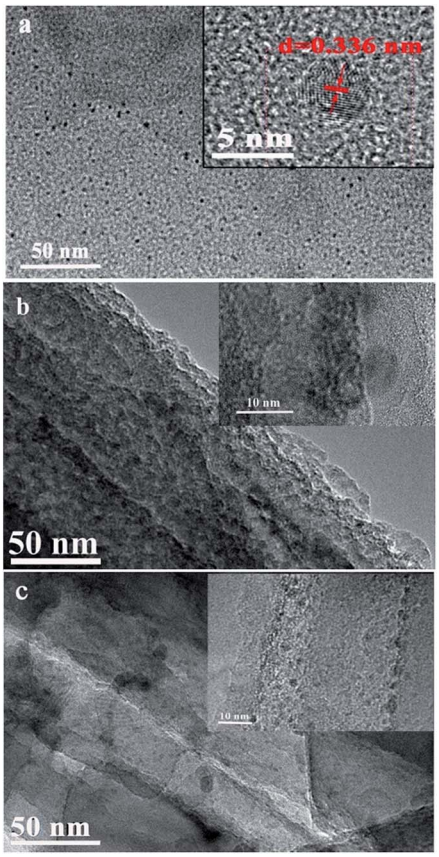

Fig. 3 TEM images of (a) g-C_3N_4 QDs (inset: HRTEM image, scale bar: 5 nm), (b) pristine SiNWs (inset: HRTEM image, scale bar: 10 nm), (c) SiNWs@g-C_3N_4 QDs (inset: HRTEM image, scale bar: 10 nm).

The surface chemical composition and oxidation state of SiNWs@g-C_3N_4 QDs composites were characterized using X-ray photoelectron spectroscopy (XPS). Fig. 4a showed the survey XPS spectra of SiNWs@g-C_3N_4 QDs. The existence of Si 2p, O 1s, C 1s and N 1s indicated that the sample was composed of Si, O, C and N elements. The high-resolution Si 2p spectrum of SiNWs@g-C_3N_4 QDs was displayed in Fig. 4b. Two deconvolution peaks at binding energies of 99.0 eV and 103.1 eV corresponded to Si atoms from Si and SiO_2, respectively. The presence of SiO_2 indicated that g-C_3N_4 QDs layer on SiNW was not continuous and part surface of SiNW was uncovered by g-C_3N_4 QDs. This result was accordant to the TEM observation (Fig. 3c). The C 1s spectrum of SiNWs@g-C_3N_4 QDs (Fig. 4c) showed three peaks. The major peak at 284.9 eV was assigned to C atoms in C–C bond or adventitious carbon in the turbostratic CN structure. The second peak at 286.5 eV was attributed to the C–N–C or formation of C–OH functional groups.[24] The peak at 288.0 eV corresponded to the sp^2 C atoms bonded to N(N–C=N) in aromatic rings.[25] Fig. 4d depicted the spectrum of N 1s for SiNWs@g-C_3N_4 QDs. The N 1s spectrum displayed two main peaks at 400 eV and 401.5 eV, originating from tertiary N in N–$(C)_3$ groups and N atoms in –NH_2 or =NH terminal amino groups,[26] respectively. In addition, the presence of the N–$(C)_3$ group confirmed the polymerization of melamine. Comprehensive analysis of XPS results proved that the sample was composed of g-C_3N_4 and Si.

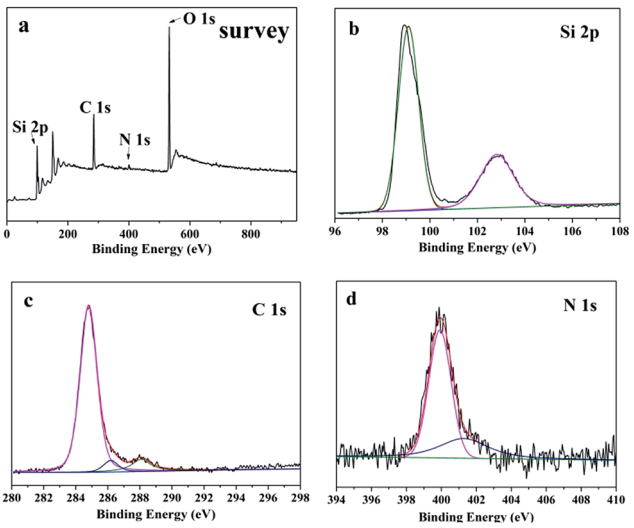

Fig. 4 XPS analysis of SiNWs@g-C_3N_4 QDs composites: (a) survey spectra, (b–d) high resolution Si 2p, C 1s and N 1s spectra.

3.2 Photoelectrochemical performance

The PEC performances of SiNWs and SiNWs@g-C_3N_4 QDs as photocathodes were estimated in 0.5 M H_2SO_4 solution under Xe lamp irradiation. Fig. 5a displayed the linear sweep voltammetry curves of SiNWs with different lengths. Obviously, the photocurrent densities of SiNWs increased from 2.6 mA cm^{-2} to 4.2 mA cm^{-2} as the length increased from 0.5 μm to 2 μm (Fig. 5a). When continuing to prolong the length to 7 μm, the photocurrent began to decline. The reduction of the photocurrent with the prolonged length of the pristine Si nanowires may be aroused from multiple reasons. First, the photon penetration depth for Si materials was constant. Once the length of SiNW exceeded the value, there were no more photogenerated charges appeared. Meanwhile, some nanowire might break away from Si wafer with the further increase of the SiNW length, resulting in the reduced density of nanowire distribution and subsequently the impaired optical absorption.[27] What's more, for longer SiNW, the photogenerated charges coming from the top of nanowire had to travel longer distance to reach Si substrate, leading to the more chance for recombination. The result indicated that SiNWs-2 showed favorable chemical stability and the most excellent PEC performance. Therefore, the sample of SiNWs-2 was chosen for the following experiment. Fig. 5b showed that the photocurrent of SiNWs@g-C_3N_4 QDs was up to 6.7 mA cm^{-2} at −1.5 V (*vs.* SCE), which was 1.6-fold than that of SiNW-2. The superior behavior may be attributed to the improved charge separation ability resulting from the build-in electric field in the interface between SiNW and g-C_3N_4 QDs. Furthermore, the photostability of SiNWs@g-C_3N_4 QDs was evaluated by cyclic voltammetry measurements. As shown in Fig. 5c, during 10 circles of cyclic voltammetry measurements, the photocurrent of SiNWs electrode attenuated gradually, which was ascribed to inhibition of the charge transfer resulting from an insulated SiO_2 layer grown on the surface of SiNWs.

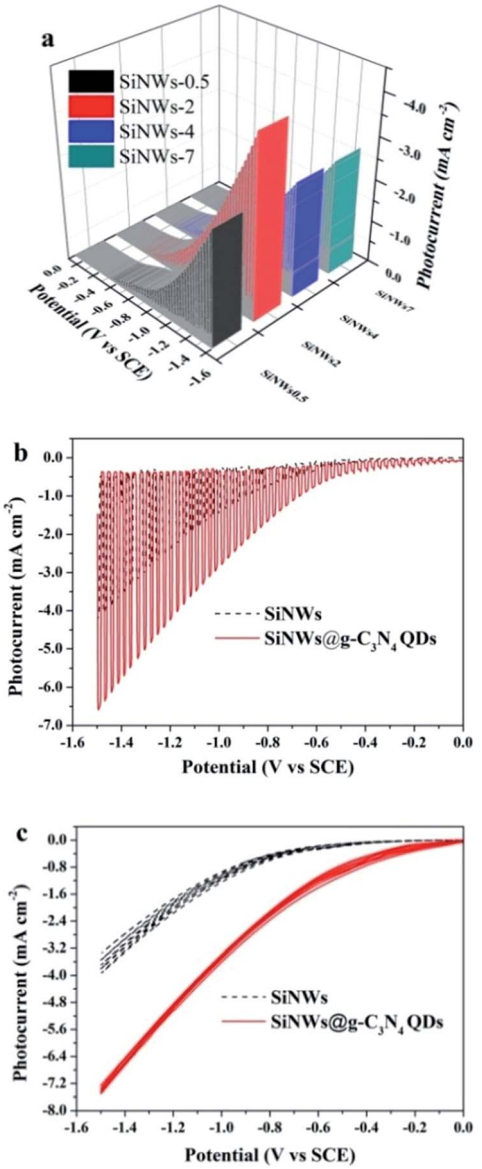

Fig. 5 Photoelectrochemical properties: (a) *I*–*V* curves of SiNWs photocathodes with various etching times; (b) *I*–*V* curves of SiNWs and SiNWs@*g*-C_3N_4 QDs photocathodes and (c) 10 cycles of cyclic voltammetry curves of SiNWs and SiNWs@*g*-C_3N_4 QDs photocathodes in 0.5 M H_2SO_4 solution under xenon lamp illumination (100 mW cm^{-2}).

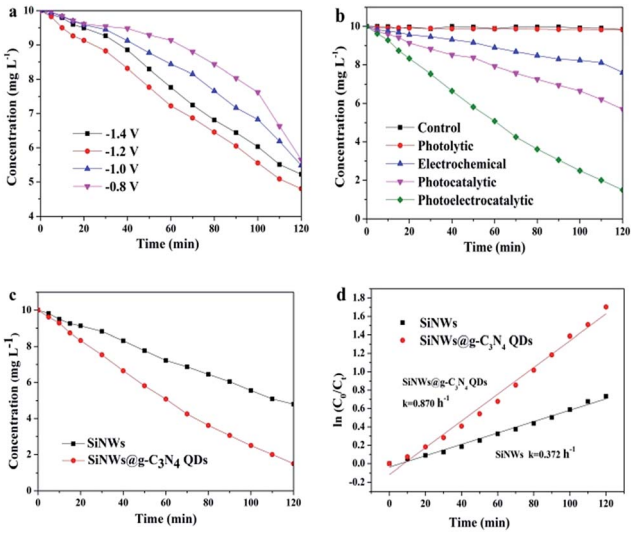

Fig. 6 Photoelectrocatalytic degradation of 4-chlorophenol (C_0 = 10 mg L^{-1}) (a) with different bias (−1.4 V, −1.2 V, −1.0 V, −0.8 V *vs.* SCE) using SiNWs; (b) with different process using SiNWs@*g*-C_3N_4 QDs photocathode (−1.2 V *vs.* SCE); (c) using SiNWs and SiNWs@*g*-C_3N_4 QDs photocathodes (−1.2 V *vs.* SCE) under visible light irradiation (λ > 400 nm, I = 100 mW cm^{-2}); (d) kinetic constants of (c).

While for SiNWs@*g*-C_3N_4 QDs, the photocurrent remained stable after 10 cycles (Fig. 5c), indicating that the layer of *g*-C_3N_4 QDs could protect Si electrode from photocorrosion in aqueous solutions. The above results suggested that *g*-C_3N_4 QDs coated on the surface of SiNWs could improve the stability of SiNWs photocathode, which brought out improved PEC ability.

3.3 Photoelectrocatalytic activity

The degradation of 4-chlorophenol experiments were carried out to further investigate the photoelectrocatalytic activity of SiNWs@*g*-C_3N_4 QDs. Fig. 6a displayed the photoelectrocatalytic degradation of 4-chlorophenol over SiNWs under various bias. It was found that the degradation efficiency increased with the bias increased from −0.8 V to −1.2 V, and then decreased as the bias further increased to −1.4 V, possibly due to the water splitting into hydrogen process under higher potential rather than degradation of 4-chlorophenol. Accordingly, SiNWs showed the highest degradation efficiency with −1.2 V bias *vs.* SCE. Thus the bias of −1.2 V *vs.* SCE was chosen for the following experiments.

As control, the degradations of 4-chlorophenol on SiNWs@*g*-C_3N_4 QDs in the various processes were also studied including the dark control, the direct photolytic, electrochemical and photocatalytic process as shown in Fig. 6b. The degradation efficiency in dark and photolytic process were insignificant, also it reached only 24.0% and 43.0% in electrochemical process and photocatalytic process after 120 min, respectively. Significantly, 85.1% of degradation efficiency was achieved in photoelectrocatalytic process, which indicated clearly that photoelectrocatalytic process was the most efficient approach to degrade 4-chlorophenol.

Fig. 6c was photoelectrocatalytic degradation comparisons using pristine SiNWs and SiNWs@*g*-C_3N_4 QDs as photocathodes, respectively. It was obvious that only 52.0% of 4-chlorophenol was degraded using SiNWs, while 85.1% of 4-chlorophenol was degraded using SiNWs@*g*-C_3N_4 QDs after 120 min. The degradation rates of 4-chlorophenol on SiNWs and SiNWs@*g*-C_3N_4 QDs photocathodes were found to follow pseudo-first-order kinetics, and their kinetics constants were presented in Fig. 6d. It was found that the kinetics constant of SiNWs@*g*-C_3N_4 QDs (0.870 h^{-1}) was calculated to be 2.3-fold than that of pristine SiNWs (0.372 h^{-1}). The 4-chlorophenol degradation results proved the fact that decoration of SiNWs by *g*-C_3N_4 QDs could successfully reduce the photocorrosion and improve photoelectrocatalytic activity of SiNWs efficiently.

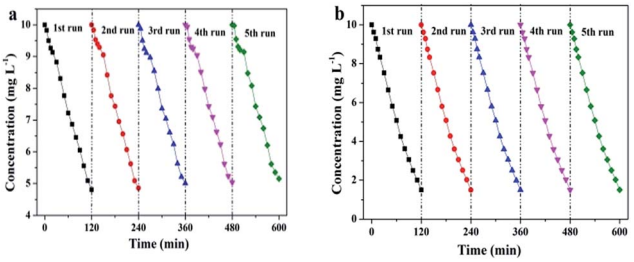

Fig. 7 Consecutive runs in the photoelectrocatalytic degradation of 4-chlorophenol (C_0 = 10 mg L^{-1}) for (a) SiNWs photocathode and (b) SiNWs@g-C_3N_4 QDs photocathode (−1.2 V *vs.* SCE) under visible light irradiation (λ > 400 nm, I = 100 mW cm^{-2}).

Furthermore, we investigated the photoelectrocatalytic stability of SiNWs and SiNWs@g-C_3N_4 QDs. Repeated photoelectrocatalytic degradation experiments were carried out to degrade 4-chlorophenol under the same condition and cycled for five times. As shown in Fig. 7a, over five consecutive cycles, ~4% decrease of degradation efficiency was obtained using SiNWs photocathode. Surprisingly, there was almost no significant deactivation observed using SiNWs@g-C_3N_4 QDs photocathode (Fig. 7b), indicating the high stability of the SiNWs@g-C_3N_4 QDs in the photoelectrocatalytic process for 4-chlorophenol degradation. The vigorous stability mainly benefited from the role of g-C_3N_4 QDs protective layer on the surface of SiNWs. In addition, nanopores (shown in Fig. 3c) built on the surface of SiNWs@g-C_3N_4 QDs could also play a minor role to inhibit the oxidation passivation.[22]

4. Conclusions

In summary, we have successfully fabricated SiNWs@g-C_3N_4 QDs composite. The prepared composite was proved to have an enhanced photostability and PEC performance due to the excellent protective performance of g-C_3N_4 QDs deposited. The experimental results suggested that the photocurrent of optimal SiNWs@g-C_3N_4 QDs was 1.6 times as much as that of bare SiNWs, which was attributed to the improved photogenerated charge separation. The photoelectrocatalytic activity for degradation of 4-chlorophenol also showed a remarkable enhancement under visible irradiation than that of SiNWs. The fabricated SiNWs@g-C_3N_4 QDs with improved optical stability and efficient charge separation are promising to be a candidate for solar energy conversion.

Acknowledgements

This work was financially supported by National Natural Science Foundation of China (No. 21377020) and Program for Liaoning Excellent Talents in University (LJQ2014008).

Notes and references

1 R. Liu, C. Stephani, J. J. Han, K. L. Tan and D. Wang, *Angew. Chem., Int. Ed.*, 2013, **52**, 4225–4228.
2 J. Oh, T. G. Deutsch, H. Yuan and H. M. Branz, *Energy Environ. Sci.*, 2011, **4**, 1690–1694.
3 A. Bansal and N. S. Lewis, *J. Phys. Chem. B*, 1998, **102**, 4058–4060.
4 N. Massad-Ivanir, G. Shtenberg, T. Zeidman and E. Segal, *Adv. Funct. Mater.*, 2010, **20**, 2269–2277.
5 H. Meng, K. Fan, J. Low and J. Yu, *Dalton Trans.*, 2016, **45**, 13717–13725.
6 Z. Huang, P. Zhong, C. Wang, X. Zhang and C. Zhang, *ACS Appl. Mater. Interfaces*, 2013, **5**, 1961–1966.
7 T. Yu, F. Wang, Y. Xu, L. Ma, X. Pi and D. Yang, *Adv. Mater.*, 2016, **28**, 4912–4919.
8 V. C. S. Tony, C. H. Voon, C. C. Lee, B. Y. Lim, M. K. M. Arshad, S. C. B. Gopinath, K. L. Foo, A. R. Ruslinda, U. Hashim and M. N. Nashaain, *Ceram. Int.*, 2016, **42**, 17642–17649.
9 Y. Du, H. Zheng and H. Ni, *J. Mater. Sci.*, 2016, **22**, 209–212.
10 Z. Xiong, M. Zheng, H. Li, L. Ma and W. Shen, *Mater. Lett.*, 2013, **112**, 211–214.
11 Y. He, Y. Zhong, F. Peng, X. Wei, Y. Su, S. Su, W. Gu, L. Liao and S. Lee, *Angew. Chem., Int. Ed.*, 2011, **50**, 3080–3083.
12 J. E. Allen, E. R. Hemesath, D. E. Perea, J. L. Lensch-Falk, Z. Y. Li, F. Yin, M. H. Gass, P. Wang, A. L. Bleloch, R. E. Palmer and L. J. Lauhon, *Nat. Nanotechnol.*, 2008, **3**, 168–173.
13 R. Chen, D. Li, H. Hu, Y. Zhao, Y. Wang, N. Wong, S. Wang, Y. Zhang, J. Hu, Z. Shen and Q. Xiong, *J. Phys. Chem. C*, 2012, **116**, 4416–4422.
14 M. Lv, S. Su, Y. He, Q. Huang, W. Hu, D. Li, C. Fan and S. Lee, *Adv. Mater.*, 2010, **22**, 5463–5467.
15 Z. Peng, H. Hu, M. I. B. Utama, L. M. Wong, K. Ghosh, R. Chen, S. Wang, Z. Shen and Q. Xiong, *Nano Lett.*, 2010, **10**, 3940–3947.
16 K. Peng, X. Wang, X. Wu and S. Lee, *Nano Lett.*, 2009, **9**, 3704–3709.
17 Y. Zheng, J. Liu, J. Liang, M. Jaroniec and S. Z. Qiao, *Energy Environ. Sci.*, 2012, **5**, 6717–6731.
18 J. Liu, T. Zhang, Z. Wang, G. Dawsona and W. Chen, *J. Mater. Chem.*, 2011, **38**, 14398–14401.
19 B. Wang, H. Yu, X. Quan and S. Chen, *Mater. Res. Bull.*, 2014, **59**, 179–184.
20 W. Wang, J. C. Yu, Z. Shen, D. K. L. Chan and T. Gu, *Chem. Commun.*, 2014, **50**, 10148.
21 K. Peng, Y. Yan, S. Gao and J. Zhu, *Adv. Funct. Mater.*, 2003, **13**, 127–132.
22 S. Wu, H. Yu, N. Lu, X. Quan and S. Chen, *Sep. Purif. Technol.*, 2017, **175**, 454–459.
23 X. Zhang, H. Wang, H. Wang, Q. Zhang, J. Xie, Y. Tian, J. Wang and Y. Xie, *Adv. Mater.*, 2014, **26**, 4438–4443.
24 M. Lublow, A. Fischer, C. Merschjann, F. Yang, T. Schedel-Niedrig, J. F. Veyan and Y. J. Chabal, *J. Mater. Chem. A*, 2014, **2**, 12697.
25 N. Boonprakob, N. Wetchakun, S. Phanichphant, D. Waxler, P. Sherrell, A. Nattestad, J. Chen and B. Inceesungvorn, *J. Colloid Interface Sci.*, 2014, **417**, 402–409.
26 M. Fu, J. Pi, F. Dong, Q. Duan and H. Guo, *Int. J. Photoenergy*, 2013, **2013**, 1–7.
27 H. Yu, F. Fan, S. Wu, H. Zhang, N. Lu, X. Quan, S. Chen and H. Li, *RSC Adv.*, 2016, **6**, 78564–78569.